Mecánica Computacional Vol. XXI, pp. 1213–1231
S. R. Idelsohn, V. E. Sonzogni and A. Cardona (Eds.)
Santa Fe–Paraná, Argentina, October 2002

AN EDGE-BASED UNSTRUCTURED FINITE VOLUME METHOD FOR THE SOLUTION OF POTENTIAL PROBLEMS

Paulo R. M. Lyra, Rita de C. F. de Lima*, Carla S. C. Guimarães and Darlan K. E. de Carvalho

Departamento de Engenharia Mecânica – UFPE
Av. Acadêmico Hélio Ramos, S/N
Recife/PE, CEP 50740-530 - Brasil
*ritalima@npd.ufpe.br
FAX: (081) 32718704

Key words: Finite Volume Method, Unstructured Mesh, Edge Based Data Structure, Potential Problems.

Abstract. *The FV formulation is very flexible to deal with any kind of control volume and so any kind of unstructured meshes, including triangular, quadrilateral, mixed or even dual meshes. The element-based finite volume methods are usually either a node/vertex centered, where the unknowns are defined at the nodes of the mesh, or element/cell centered where the unknowns are defined within the element, usually at the element centroid. Both options have advantages and disadvantages, but in two-dimensional applications all of them have basically the same computational cost, which is proportional to the number of edges of the mesh. However, the node-centered formulation has a strong connection with an edge-based finite element formulation, when linear triangular elements are used, and requires less memory and computations when extended for three-dimensional tetrahedral meshes. In this article an unstructured finite volume node centered formulation, implemented using an edge-based data structure, is adapted and detailed for the solution of two-dimensional potential problems. The whole formulation is fully described considering triangular meshes, but it can directly be extended and applied to any conform two-dimensional meshes. A straight extension for three-dimension is also possible but not attempted here. In order to demonstrate the potentiality of the presented procedure some model problems are investigated.*

1 INTRODUCTION

Whenever analyzing numerical applications that involves complex geometries, the adoption of methods able to deal with unstructured meshes is very attractive and highly recommended[1]. Within such class of methods the most frequently used are the finite element method (FEM)[17] and the finite volume method (FVM)[3]. The cell vertex finite volume formulation using median dual control volumes is implemented using an edge-based data structure and is adapted and detailed for solving two-dimensional potential problems. This finite volume formulation is very flexible and efficient, and it is equivalent to the edge-based FEM when linear triangular elements are employed[1,7,14]. The formulation is flexible to deal with any kind of unstructured meshes without making any distinction. For instance, in 2-D triangular, quadrilateral or mixed meshes can be directly used, and the same happens when dealing with 3-D, where tetrahedral, hexahedral, pyramids, prisms and mixed meshes can be adopted. In terms of efficiency both memory and CPU time requirements are reduced by using an edge-based implementation[3,14,15]. Finally, edge-based data structure allows for the implementation of different types of finite difference discretization in the context of 2-D and 3-D unstructured meshes[7,8,12].

This paper presents FV discretization of a transient potential problem subject to all sort of boundary conditions (Dirichlet, Neumann, and Cauchy), some non-conventional loads and applied to problems involving multi-materials. The developed computational system is very flexible and it is intended to be used on the simulation of bioheat transfer applications[6]. After this introduction remarks, the physical-mathematical model considered is described. Then, the discrete formulation is fully presented, involving the spatial and time approximations adopted. Some important implementation aspects are discussed and several simple model problems are analyzed to validate and to study the performance of the whole procedure. Finally, some concluding comments are presented and the potentiality of the described approach is highlighted.

2 GOVERNING EQUATIONS

Using the energy conservation law we can derive the partial differential equation that governs transient heat transfer in a stationary continuous medium,

$$\rho c \frac{\partial T}{\partial t} = \frac{\partial q_j}{\partial x_j} + S \qquad in \quad \Omega \; X \; \mathbf{T} \tag{1}$$

which is a classical example of a potential problem. In previous equation, $C = \rho c$ is the heat capacity, with ρ being the mass density and c being the specific heat, T is the temperature, q_j is the heat flux in x_j direction and S represents the source (or sink) terms. The spatial domain of the problem is represented by Ω, with x_j being the spatial independent variable with j varying from one to the number of spatial dimensions, and $\mathbf{T} = [t^i, t^f]$ represents the time interval of integration.

The constitutive relation between the conductive heat flux and the temperature gradients are given by Fourier's law,

$$q_j = -k_j \frac{\partial T}{\partial x_j} \tag{2}$$

where k_j is the thermal conductivity in x_j direction. For simplicity, the medium is considered orthotropic with ρ, c, k_j constants and (1) represents a linear non-homogeneous parabolic second-order partial differential equation.

Equation (1) represents a boundary-initial value problem and must be subjected to boundary and initial conditions. The boundary conditions of interest can be of different types.

a) A prescribed temperature $\overline{T}$ over a portion of the boundary Γ_D, i.e. Dirichlet boundary condition:

$$T = \overline{T} \qquad in \quad \Gamma_D \; X \, \mathbf{T} \tag{3}$$

b) A prescribed normal heat flux $\overline{q}_n$ over Γ_N, also known as Neumann boundary condition:

$$-q_j n_j = \overline{q}_n \qquad in \quad \Gamma_N \; X \, \mathbf{T} \tag{4}$$

in which n_j is the outward normal direction cosines.

c) A mixed type boundary condition over Γ_C, called Cauchy or Robin boundary condition:

$$-q_j n_j = \overline{q}_n + \alpha_\Gamma (T - T_a) \qquad in \quad \Gamma_R \; X \, \mathbf{T} \tag{5}$$

where α_Γ is the film coefficient and T_a is the bulk fluid temperature.

Finally, an initial distribution of the temperature $\overline{T}^i$ must be known at an initial time stage t^i, and the initial condition is expressed by

$$T = \overline{T}^i \qquad in \quad \Omega \quad and \quad t = t^i \tag{6}$$

Equations (1) to (6) fully describe our mathematical model, which governs heat conduction in a stationary medium.

3 FINITE VOLUME FORMULATION

In this section most of the numerical formulation adopted is presented without reference to a particular type of mesh or spatial dimension. Later the formulation is completed by assuming a two dimensional computational domain discretized into an unstructured assembly of triangular elements. The time discretization adopted is the simple first-order accurate Euler-forward scheme, which is also presented for completeness.

3.1 Spatial discretization

The integral form of the potential problem given by eq. (1) is written as

$$\int_{\Omega} \rho c \frac{\partial T}{\partial t} d\Omega = \int_{\Omega} \frac{\partial q_j}{\partial x_j} d\Omega + \int_{\Omega} S d\Omega \tag{7}$$

or alternatively by the use of the divergent theorem,

$$\int_{\Omega} \rho c \frac{\partial T}{\partial t} d\Omega = \int_{\Gamma} q_j n_j d\Gamma + \int_{\Omega} S d\Omega \tag{8}$$

where Ω denotes an arbitrary control volume, with closed boundary Γ .

The computational domain is discretized into an unstructured assembly of elements. Then equation (8) is applied over each control volume in the mesh. So the volume integrals of (8) can be computed over the control volume surrounding node *I* as

$$\rho c \int_{\Omega_I} \frac{\partial T}{\partial t} d\Omega \cong \rho c \frac{\partial T_I}{\partial t} V_I \cong \rho c \frac{\partial \hat{T}_I}{\partial t} V_I \tag{9}$$

and

$$\int_{\Omega_I} S d\Omega \cong S_I V_I \tag{10}$$

where V_I is the volume of the control volume, $\hat{T}_I$ and S_I represent the numerical calculated temperature and source term at node *I*, respectively.

The boundary integral presented in equation (8) is computed over the boundary of the control volume that surrounds node *I* using an edge-based representation of the mesh, i.e.

$$\int_{\Gamma_I} q_j n_j d\Gamma \cong \sum_{L} C^j_{IJ_L} q^{j(\Omega)}_{IJ_L} + \sum_{L} D^j_{IJ_L} q^{j(\Gamma)}_{IJ_L} \tag{11}$$

for a general flux q_j. In equation (11) $C^j_{IJ_L}$ denotes the coefficient that must be applied to the edge value of the flux $q^{j(\Omega)}_{IJ_L}$ in the x_j direction to obtain the contribution made by the edge to node *I*. In addition, $D^j_{IJ_L}$ represents the boundary edges coefficients that must be applied to the boundary edge flux $q^{j(\Gamma)}_{IJ_L}$ when the edge *L* lies on the boundary. These coefficients can be readily computed and this will be detailed afterwards. The first summation in eq. (11) extends over all edges *L* in the mesh which are connected to node *I*, and the second summation is only non-zero when node *I* is on the boundary and extends over all boundary edges that are connected to node *I*.

By considering the approximations given by eqs. (9), (10) and (11), the semi-discrete formulation of equation (8) can be conveniently expressed as

$$\rho c_p \frac{d\hat{T}_I}{dt} V_I = \sum_L C^j_{IJ_L} q^{j(\Omega)}_{IJ_L} + \sum_L D^j_{IJ_L} q^{j(\Gamma)}_{IJ_L} + S_I V_I \tag{12}$$

The approximation of the value of the edge flux $q^{j(\Omega)}_{IJ_L}$ is computed using the midpoint rule, or simple arithmetic average

$$q^{j(\Omega)}_{IJ_L} = \frac{q^j_I + q^j_{J_L}}{2} \tag{13}$$

Several alternatives can be adopted to compute $q^{j(\Gamma)}_{IJ_L}$. The adopted one considers a linear variation of the flux over edge IJ_L. It is given by

$$q^{j(\Gamma)}_{IJ_L} = \frac{\left(3q^j_I + q^j_{J_L}\right)}{4} \tag{14}$$

In order to compute the edge flux described by eqs. (13) and (14) we need to know the nodal values of the fluxes and so the nodal values of temperature gradients. By adopting the divergence theorem and the approximation used to compute volume integrals over a control volume surrounding node I, we have

$$\int_{\Omega_I} \frac{\partial T}{\partial x_j} d\Omega = \int_{\Gamma_I} T n_j d\Gamma \qquad \text{and} \qquad \int_{\Omega_I} \frac{\partial T}{\partial x_j} d\Omega \cong \frac{\partial T}{\partial x_j} V_I \tag{15}$$

From previous expressions and using the same approximation adopted to compute the boundary integral in equation (11), we get the approximate nodal gradients through

$$\frac{\partial T_I}{\partial x_j} V_I \cong \int_{\Gamma_I} T n_j d\Gamma \cong \sum_L C^j_{IJ_L} T^{(\Omega)}_{IJ_L} + \sum_L D^j_{IJ_L} T^{(\Gamma)}_{IJ_L} \tag{16}$$

The edge values of the temperature, $T^{(\Omega)}_{IJ_L}$ and $T^{(\Gamma)}_{IJ_L}$, are calculated by

$$\begin{aligned} T^{(\Omega)}_{IJ_L} &= \frac{T_I + T_{J_L}}{2} \\ T^{(\Gamma)}_{IJ_L} &= \frac{\left(3T_I + T_{J_L}\right)}{4} \end{aligned} \tag{17}$$

The use of expression (16) to compute the gradients implies that the discretization of the diffusion term in eq. (12) involves information from two layers of points surrounding the point I under consideration. Furthermore, if an uniform structured quadrilateral (or hexahedral) mesh is adopted, the values computed at a given node are uncoupled from the values of those nodes directly connected to it. This fact may leads to "checker-boarding" or "odd-even" oscillations[7,14]. When computing the diffusive term in non-uniform unstructured meshes, the adoption of an extended stencil and a weak coupling with the directly connected nodes may lead to some loss of robustness and reduction on convergence rate of the resulting scheme. To overcome shuch weaknesses, the gradients must be computed in an alternative way. Following the procedure suggested in the literature[4,14] a better approach can be developed as follows.

The edges values of the temperature gradient can be approximately computed by

$$\frac{\partial T_{IJ_L}}{\partial x_j} \cong \frac{\partial \hat{T}_{IJ_L}}{\partial x_j} = \frac{1}{2}\left(\frac{\partial \hat{T}_I}{\partial x_j} + \frac{\partial \hat{T}_{J_L}}{\partial x_j}\right) \tag{18}$$

Using a local frame of reference, in which one axis is along the edge (direction P) and another axis is in the orthogonal plane (N) to direction (P), (see figure 1), the edge gradient can be alternatively computed as

$$\frac{\partial \hat{T}_{IJ_L}}{\partial x_j} = \frac{\partial \hat{T}^P_{IJ_L}}{\partial x_j} + \frac{\partial \hat{T}^N_{IJ_L}}{\partial x_j} \tag{19}$$

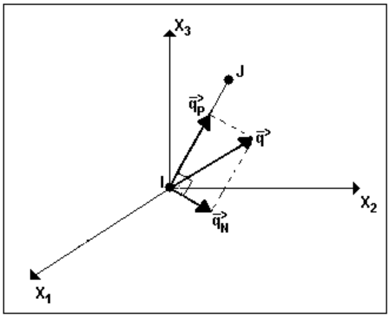

Figure 1: Local frame of reference

Once the nodal gradients are known the corresponding fluxes can be directly obtained using the Fourier Constitutive Law (2). Similarly the edge fluxes are given by

$$q^{j(\Omega)}_{IJ_L} = \frac{\left(q^j_I + q^j_{J_L}\right)}{2} = \left(q^{j(\Omega)}_{IJ_L}\Big|_P + q^{j(\Omega)}_{IJ_L}\Big|_N\right) \tag{20}$$

Using a central finite difference second-order approximation, the temperature derivative over the edge direction (P) can be calculated by

$$\frac{\partial \hat{T}_{IJ_L}}{\partial x_{P^*}} = \frac{\hat{T}_{J_L} - \hat{T}_I}{\Delta X_{IJ_L}} \boldsymbol{L}_{IJ_L} \tag{21}$$

where the superscript * is adopted to distinguish from the same term computed using the finite volume approximation described previously by equation (16). In equation (21) we have

$$\Delta X_{IJ_L} = \left| \boldsymbol{X}_{J_L} - \boldsymbol{X}_I \right| \qquad \text{with} \qquad \boldsymbol{X}_I = \left(x_I^1, x_I^2 \right) \tag{22}$$

and

$$\boldsymbol{L} = \boldsymbol{L}_{IJ_L} = \frac{\boldsymbol{X}_{J_L} - \boldsymbol{X}_I}{\Delta X_{IJ_L}} \qquad \text{and} \qquad L_j = \frac{x_{J_L}^j - x_I^j}{\Delta X_{IJ_L}} \tag{23}$$

where $\boldsymbol{L}$ represents the unitary vector defined in the edge direction from I to J_L, and L_j are the director cosines.

The cartesian components of the derivative on the edge direction are given by

$$\frac{\partial \hat{T}_{IJ_L}^{P^*}}{\partial x_j} = L_j \frac{\partial \hat{T}_{IJ_L}}{\partial x_{P^*}} \tag{24}$$

and the Cartesian components of the portion of the gradient orthogonal (or normal) to the edge direction is then

$$\frac{\partial \hat{T}_{IJ_L}^N}{\partial x_j} = \frac{\partial \hat{T}_{IJ_L}}{\partial x_j} - \frac{\partial \hat{T}_{IJ_L}^P}{\partial x_j} = N_j \frac{\partial \hat{T}_{IJ_L}}{\partial x_N} = N_j \frac{\partial \hat{T}_{IJ_L}}{\partial x_K} N_K \tag{25}$$

where $\partial \hat{T}_{IJ_L} / \partial x_K$ is computed in a finite volume fashion given by eq. (16), and N_K represents the director cosines of the component of the total gradient in the direction normal to the edge direction.

To summarize, the edge temperature gradient given by (19) is computed using the edge direction quantity calculated as given by (24) and the normal one using (25). Similarly, the edge fluxes components given by (20) are now replaced by (26), which are computed using the gradients as described previously and the Fourier Constitutive Law (2), i.e.

$$q_{IJ_L}^{j(\Omega^*)} = \frac{\left(q_I^j + q_{J_L}^j \right)}{2} \cong \left(q_{IJ_L}^{j(\Omega)} \Big|_{P^*} + q_{IJ_L}^{j(\Omega)} \Big|_N \right) \tag{26}$$

where the heat fluxes in the edge direction $q_{IJ_L}^{j(\Omega)} \Big|_P$ are replaced by $q_{IJ_L}^{j(\Omega)} \Big|_{P^*}$.

The final semi-discrete scheme is then given by equation (12), by replacing $q_{IJ_L}^{j(\Omega)}$ with $q_{IJ_L}^{j(\Omega^*)}$, i.e.

$$\rho c_p \frac{d\hat{T}_I}{dt} V_I = \sum_L C_{IJ_L}^j q_{IJ_L}^{j(\Omega^*)} + \sum_L D_{IJ_L}^j q_{IJ_L}^{j(\Gamma)} + S_I V_I \tag{27}$$

For two-dimensional problems, the equation (8) is first integrated over x_3 and then over a 2-D space. In such model, we have the nodal volume computed as $V_I = A_I E_I$, where E_I refers to the thickness of the domain at point I, and A_I is the area of the control volume. The 2-D weighting coefficients $C^j_{IJ_L}$ and $D^j_{IJ_L}$ are defined by

$$\begin{aligned} C^j_{IJ_L} &= \sum_k A_K n^j_K \\ D^j_{IJ_L} &= A_L n^j_L \end{aligned} \tag{28}$$

where $A_K = L_K E_K$ with $E_K = \left(E_I + E_{J_L}\right)/2$ and L_K is the length of each interface K associated to edge IJ_L. Each interface connects the element centroid (C) to the middle point (MP) of one of the edges that belongs to such element. $A_L = L_L E_L$, where L_L is half the size of the boundary edge under consideration and E_L is similar to E_k defined previously. The geometric parameters required to compute the weighting coefficients are detailed in figures 2 and 3.

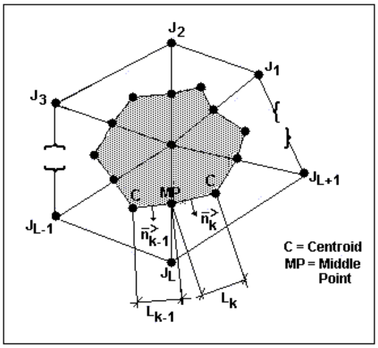

Figure 2: 2-D control volume and its geometric parameters

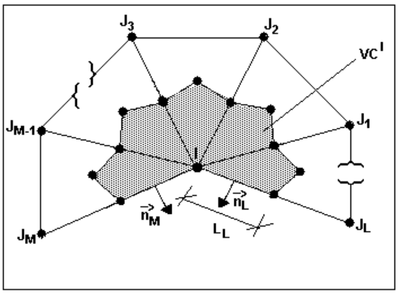

Figure 3: 2-D boundary control volume and its geometric parameters

The thermal load S over the domain, for the 2-D model, are considered here as

$$S = Q + \left[\alpha_{\Omega}\left(T_a - T\right)\right] / E \tag{29}$$

with

$$Q = Q^P + Q^C + Q^R \tag{30}$$

where the subscript P, C, R accounts for thermal sources (or "sinks") acting on a point, a curve or a region, respectively. In equation (29) the first term represents the thermal sources (or sinks) described as given in equation (30). The second term accounts for convection over each face of the two dimensional domain, α_{Ω} is the film coefficient where the subscript Ω is used to stress that it acts over the domain, while α_{Γ} in equation (5) acts over the boundary with mixed boundary condition and E is the thickness of the domain.

3.2 Loads, boundary conditions and multi-material

The discretization of the different thermal loads (equations (29) and (30)) and different boundary conditions (equations (3) to (5)) are now considered. The treatment of multi-material problems is also described here. The implementation of the discretization of certain terms exploit some flexibilities inherent on our system for bidimensional mesh generation[9]. Some of these features will be exemplified through the numerical applications presented later.

3.2.1 Thermal loads

The integral of the thermal loads Q described by (30) is given by

$$\int_{\Omega} Q d\Omega = Q^P + \int_{\Gamma_C} Q^C d\Gamma + \int_{\Omega_R} Q^R d\Omega \tag{31}$$

In eq. (31), Q^P is just a point heat source computed at a given node I, i.e. Q_I^P. If the point-source is not applied at a nodal point its value is distributed to the nodes of the triangle that contains it, using a linear approximation[10]. The flexibility of our bidimensional mesh generator[9] is the fact of building a fictitious boundary along the curve where we want to apply a line heat source per unit of area Q^C. Then the boundary integral in (31) is easily approximated by each portion of the fictitious boundary associated to node I $\left(\Gamma_{C_I}\right)$ as

$$\int_{\Gamma_{C_I}} Q^C d\Gamma \cong \sum_L Q_I^C A_L \tag{32}$$

The summation extends over the two edges connected to node I that belongs to the fictitious boundary and A_L is an area computed as previously defined.

If the heat source per unit of volume Q^R is distributed over a region Ω_R. The integral is then approximated in the same fashion as the transient term (9), i.e. for each control volume surrounding node I $\left(\Omega_{R_I}\right)$

$$\int_{\Omega_{R_I}} Q^R d\Omega \cong Q_I^R V_I \tag{33}$$

Finally, the convective type source term is computed for each Ω_{R_I} by

$$\int_{\Omega_{R_I}} \left[\alpha_{\Omega_R}(T_a - T)\right] / E \, d\Omega \cong \alpha_{\Omega_R}\left(T_a - \hat{T}_I\right) V_I / E_I \tag{34}$$

For the previous loads given in equations (33) and (34) a specific region covering Ω_R is built with the help of our mesh generator[9], which allows for the generation of consistent multi-regions meshes.

3.2.2 Boundary conditions

To compute the Dirichlet boundary condition (3), it is enough to substitute T_I by $\overline{T}_I$ whenever required, i.e. $\forall\ I \in \Gamma_D$.

To impose the Neumann boundary condition (4), the total boundary edge flux that appears in the boundary loop in equation (27) must be projected on the directions parallel and normal to the edge under consideration. The normal portion must then be replaced by the prescribed flux, $\overline{q}_n$ and the parallel portion set to zero. In order to do so, during the gradient computation we project the gradient onto the directions parallel and normal to the considered edge and by knowing the normal prescribed flux and the local thermal conductivity we also know the required gradient on the normal direction. Finally, the gradient on the normal direction is used to compute the x_j components of the flux, by simple projection and by using the constitutive Fourier relation in eq. (2).

For Cauchy boundary condition eq. (5), the value $\left(-\overline{q}_n + \alpha_\Gamma T_a\right)$ is known and computed in the same fashion as implemented to compute the Neumann boundary condition, previously described. The remaining term is computed for each Γ_{C_I} according to

$$\int_{\Gamma_{C_I}} -\alpha_\Gamma T d\Gamma \cong \sum_L \alpha_\Gamma \hat{T}_I A_L \tag{35}$$

with Γ_{C_I} being the portion of the Γ_C boundary associated to node I the summation extends over the two boundary edges connected to node I.

3.2.3 Multi-materials domain

Whenever addressing heat transfer problems which involves different material properties on different portions of the domain we need to build proper meshes for each sub-region and to perform consistently the discretization of the governing equation in order to guarantee the correct solution through the interface of the sub-regions. As already mention, our mesh generation has the flexibility to generate consistent meshes over multi-region domain.

For each edge at the interface of two regions, the edge coefficient is computed independently for each region. Referring to figure (4), the edge IJ_L would have two coefficients defined by

$$C_{IJ_L}^{j(R_1)} = A_{k-1} n_{k-1}^j \qquad and \qquad C_{IJ_L}^{j(R_2)} = A_k n_k^j \tag{36}$$

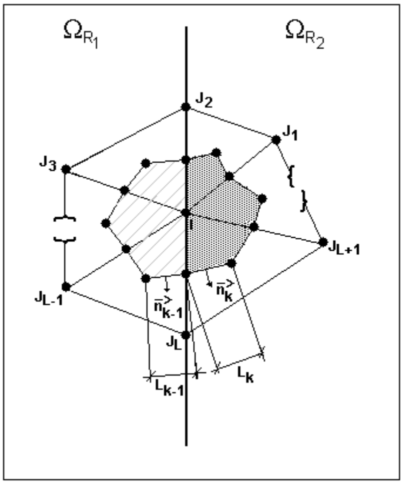

Figure 4: Control volumes at an interface between two regions and their geometric parameters

During the flux computation of we proceed a looping over each region at a time to compute the gradients and associated fluxes, using the corresponding edge coefficient and the material properties. In the computation of the "final" discrete equation, (27), we can proceed similarly looping over each region at a time, with the corresponding properties and thermal loads.

3.2.4 Some other important aspects

If the material properties, loads or boundary conditions varies in space, the middle point rule is adopted. For instance, the heat conductivity of edge IJ_L when k is a function of the spatial position is given by

$$k_{IJ_L} = \frac{k_I + k_J}{2} \tag{37}$$

If the material has non-linear behavior $\left[e.g.\ k = f(T) \right]$ is important an iterative procedure such as Newton-Raphson method must be used, but such feature was not yet attempted in the present formulation.

The adopted unstructured triangular meshes were generated with our two dimensional mesh generation system with is based upon the advancing front technique[11]. As any conventional unstructured mesh generator the mesh data consists of the physical coordinates simply listed by node numbers and a list of the connectivity of each element. Our mesh generator gives also a list of boundary edges connectivities. It is required to pre-processing the mesh data before it can be used with an edge-based finite volume solver. The pre-processing stage consists basically on: to build the arrays with the mesh and boundary topology, which are lists of edges and boundary edges with their respective connectivities, to compute and store the edge and boundary weighting coefficients; and to translate the loads and boundary conditions, which are associated to the geometry, into the mesh topological entities.

3.3 Time discretization

The semi-discrete form of the transient heat transfer problem given in equation (27) represents a coupled system of first order differential equations, which can be rewritten in a compact matrix notation as

$$\boldsymbol{M}\frac{\partial \boldsymbol{T}}{\partial t} + \boldsymbol{KT} = \boldsymbol{R} \tag{38}$$

with the initial condition given by eq. (6). In equation (38), $\boldsymbol{M}$ and $\boldsymbol{K}$ represent, respectively, the heat capacity (diagonal) matrix and $\boldsymbol{K}$ the conductivity matrix. The vector $\boldsymbol{R}$ is formed by the independent terms, which arises from the thermal loads and boundary conditions, and finally, $\boldsymbol{T}$ is the vector of the nodal unknowns. Equation (38) can be further discretized in time to produce a system of algebraic equations. With the objective of validating the finite volume formulation described, we adopted the simplest two-level explicit time step (or Euler forward scheme), which applied to equation (38) gives the following expression

$$\boldsymbol{M}\left(\frac{\boldsymbol{T}^{n+1} - \boldsymbol{T}^{n}}{\Delta t} \right) + \boldsymbol{KT}^{n} = \boldsymbol{R}^{n} \tag{39}$$

where $\Delta t = t^{n+1} - t^{n}$ is the length of the time interval and the superscripts represent the time levels. Such scheme is just first order accurate in time and the Δt must be chosen according to a stability condition[17]. Other alternatives, such as the generalized trapezoidal method[7,17], multi-stage Runge-Kutta scheme[7] or schemes involving more than two time intervals[14] can be implemented if higher-order time accuracy is required.

If an explicit time integration is adopted, both the convective source term approximated by eq. (34) and the convective boundary condition term given in eq. (35) are computed explicitly considering $\hat{T} = \hat{T}^{n}$ on the right hand side of eq. (39). If an implicit formulation were adopted the terms described in equations (34) and (35) involve the unknown $\hat{T}^{n+1}$ and would add contribution to the matrix of the final algebraic system of equations.

4 NUMERICAL RESULTS

In this section, some simple, though representative, academic examples are presented in order to show the capabilities of the numerical scheme previously discussed. Until the present moment only steady-state problems have been exploited.

4.1 Heat conduction problem in a flat plate with a distributed source term

The first and simplest academic example shown in this article presents the distribution of temperature in a square flat plate of 10m edge length and constant thickness. The four faces of the square are submitted to a temperature of T = 0.0°C and a source term of Q = 2.4 W/m^3 is distributed over the entire domain.

Figure (5) shows the isostrips of temperature for the plate and figure (6) shows the distribution of temperature through the middle of the plate (horizontal line of symmetry).

The obtained results are in excellent agreement with the numerical example presented by Hinton[5].

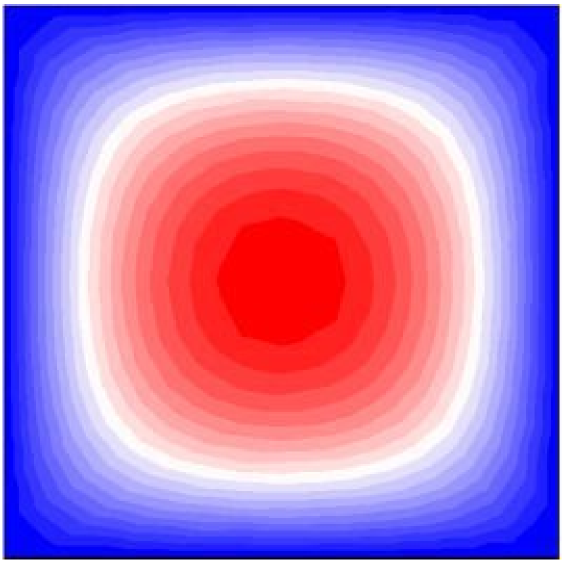

Figure 5: Isostrips of temperature for a square plate with a distributed source term over the entire domain.

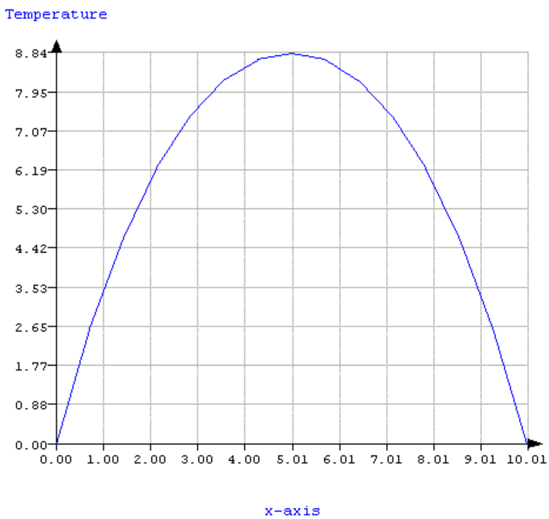

Figure 6: Distribution of temperature along middle of the plate

4.2 Steady-state heat transfer problem with convection

The second application refers to a steady state solution of a two-dimensional heat transfer problem in a rectangular plate of uniform thickness with edges of 0.6m and 1.0m length. The left face of the plate is insulated (zero heat flux), while the bottom edge is at a fixed temperature of 100°C and the right and top edges are under convection to ambient temperature of 0°C. The thermal conductivity of the plate is k = 52.0 W/m°C and the surface convective heat transfer coefficient is h = 750.0 W/m^2 °C. This example was extracted from the NEFEMS[2] selected FE benchmarks in structural and thermal analysis. The target to be achieved is a temperature of 18.3 °C in point E (see figure 7a).

In Table 1 we show the obtained results with two different meshes. The first one is a coarse mesh with 32 nodes, and the second one is a finer mesh with 793 nodes. It can be observed that the final results are in good agreement with the proposed mark. Figure (7a) shows the domain representation for this problem and figure (7b) shows the triangular coarse mesh utilized.

Table 1

TEMPERATURE AT NODE E		
NEFEMS	**Coarser Mesh**	**Finer Mesh**
18.3 °C	18.14 °C	18.29 °C

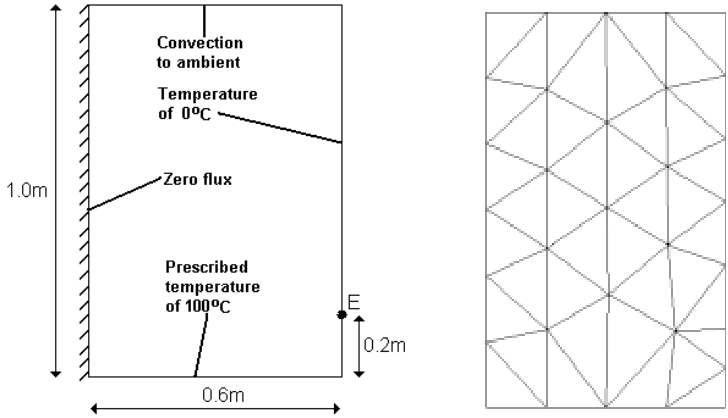

(a) (b)

Figure 7: 2-D heat transfer problem with convection: (a) domain representation; (b) coarse mesh with 32 nodes.

Figure (8) shows the isostrips of temperature for both meshes. It is important to note that even the coarse mesh provided a good result if compared with the NEFEMS[2] results. As expected, for the finer mesh, the isostrips of temperature are much smoother than those obtained with the coarser mesh.

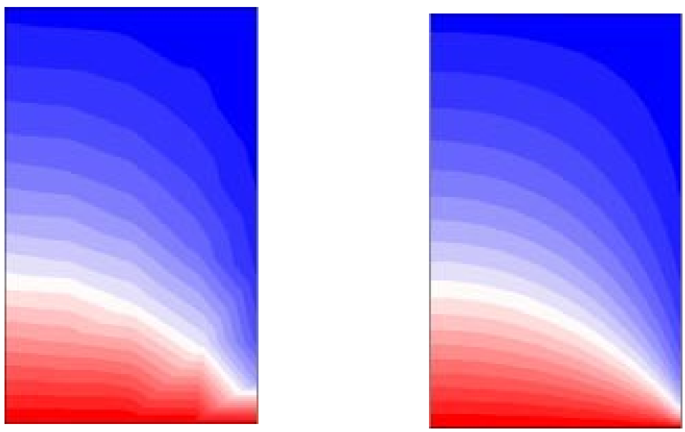

(a) (b)

Figure 8: 2-D heat transfer problem with convection: (a) Isostrips for coarser mesh (32 nodes); (b) Isostrips for finer mesh (793 nodes).

4.3 Multi-material steady-state heat conduction problem

In the final example we present a steady state problem of a rectangular plate compounded by two materials with two different conductivities. The plate of constant thickness is shown in figure (9).

The 2-D domain representing the plate was subdivided into two subdomains where the triangular mesh was built independently for each subdomain (representing each material), keeping the consistency of the mesh between them.

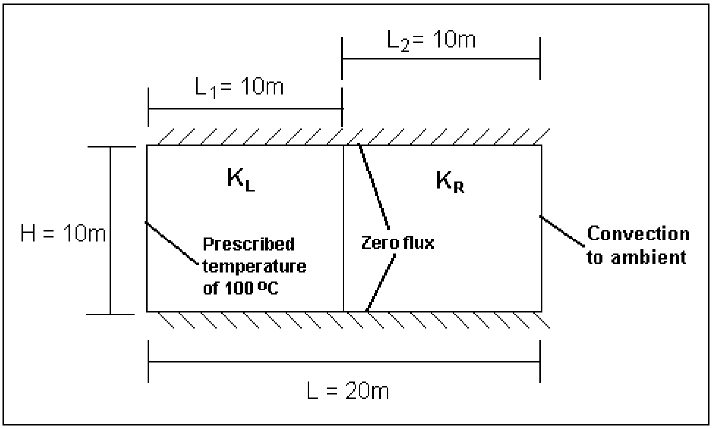

Figure 9: Domain for multi-material heat conduction problem.

The plate is submitted to a prescribed temperature (T=100 °C) on its left side and, in order to obtain an essentially 1-D problem, the top and the bottom sides of the plate are insulated. On the right side, the plate is under convection, with a convection heat transfer coefficient h = 100.0 W/m^2 °C. The conductivity of the left part of the plate ($0.0 \le x \le 10.0$) is k_L = 50.0 W/m°C, and for the right part ($10.0 \le x \le 20.0$), this coefficient is k_R = 15.0 W/m°C.

Figures 10 and 11 show, respectively, the temperature distribution for y = 0.0 and $0.0 \le x \le 20.0$, and the isostrips of temperature for this problem. The mesh utilized has 216 nodes and 410 triangles.

In figure (11), we also note the abrupt change in the slope in the curve of temperature distribution due to the change in the conductivity coefficient of the two adjacent materials.

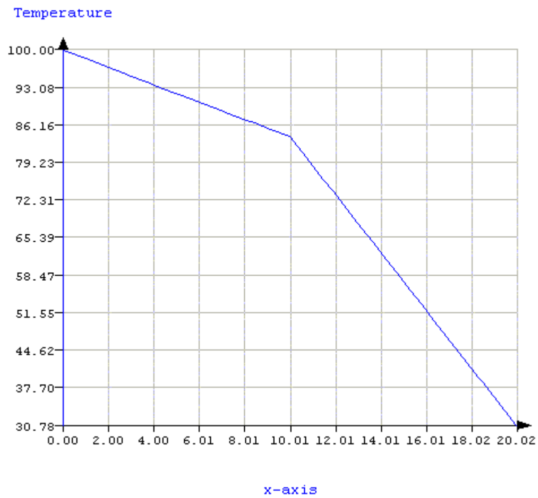

Figure 10: Temperature distribution over the y = 0.0 axis for $0.0 \leq x \leq 20.0$.

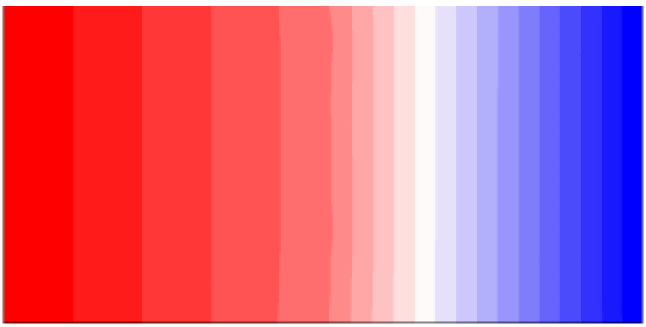

Figure 11: Isostrips for multi-material heat conduction problem.

In Table 2 we compare the nodal temperatures at the right edge and at the interface between the two different materials, with the 1-D analytical solution.

Table 2

x (m)	Analytical Solution	Numerical Solution
10 (interface)	84.03	84.04
20	30.79	30.79

5 CONCLUDING REMARKS

An unstructured finite volume formulation was fully described to deal with potential problems involving different types of boundary conditions, thermal loads and material properties. The whole system was validated for simple model state-steady problems and it seams to be promising with more complex applications. The adoption of an edge-based data structure is very flexible, easy to implement and efficient. However, the real potentiality of the developed numerical procedure must be exploited when solving more realistic problems. We plan to use our system to simulate the temperature distribution on bioheat transfer applications, such as hyperthermal treatment of inoperable tumors using laser heat sources. In these applications the flexibilities for dealing with complex geometries, multi-materials, different thermal loads and boundary conditions are of paramount importance in order to have a good model of the physical features involved in the process.

ACKNOWLEDGEMENTS

The authors would like to acknowledge the brazilian research council CNPq and the national petroleum agency (ANP) and for the financial support provided during the development of this research.

REFERENCES

[1] AGARD Report 787, "*Special course on unstructured grid methods for advection dominated flows*", France, (1992);
[2] Barlow, J. and Davies, G. A. O., "Selected FE benchmarks in structural and thermal analysis", NAFEMS (national agency for finite element methods & standards), National eng. Lab., Glasgow, U. K., (1987);
[3] Barth, T.J., "Aspects of unstructured grids and finite-volume solvers for the Euler and Navier-Stokes equations", *AGARD Report 787*, pp. 6.1-6.61, (1992);
[4] Crumpton, P.I., Moinier, P. and Giles, M.B. T.J., "An unstructured algorithm for high Reynolds number flows on highly stretched grids". In: C. Taylor and J.T. Cross, editors*, Numerical Methods In Laminar and Turbulent Flow*, pp. 561-572, Pineridge Press, (1997);
[5] Hinton, E. & Owen, D. R., *An introduction to finite element computations*, Pineridge Press, (1974);
[6] Lima, R. de C. F. de, Lyra, P.R.M. e Guimarães, C. S. C. "Uma técnica para o cálculo do campo de temperaturas em tumores abdominais pela solução da equação da biotransferência de calor através do uso do método dos volumes finitos em malhas não-estruturadas", *LATCYM2002 – Nono Congreso Latino americano de Transferencia de Calor y Materia*, Porto Rico, november, (2002), (*In Portuguese*);
[7] Lyra, P.R.M., *Unstructured grid adaptive algorithms for fluid dynamics and heat conduction*, Ph.D. thesis C/PH/182/94, University of Wales - Swansea, (1994);

[8] Lyra, P.R.M., Morgan, K.; Peraire, J. and Peiró, J., "TVD algorithms for the solution of the compressible euler equations on unstructured meshes", *International Journal for Numerical Methods in Fluids,* Vol. 19, pp. 827-847, (1994);
[9] Lyra, P.R.M and Carvalho, D.K.E., "A flexible unstructured mesh generator for transient anisotropic remeshing", *ECCOMAS 2000 – European Congress on Comp. Meth. in Applied Sciences and Eng.*, Barcelona-Espanha, september, published in CD-ROM, (2000);
[10] Lyra, P.R.M, Almeida, F.P.C., Willmersdorf, R. B., and Afonso, S.M.B., "An adaptive fem integrated system for the solution of transient thermal-structural problems", *CILAMCE 2000 - Iberian Latin American Congress on Computational Methods in Engineering*, Rio de Janeiro-Brasil, december, pp. 1-18, published in CD-ROM, (2000);
[11] Peraire, J.; Vahdati, M.; Morgan, K. and Zienkiewicz, O.C., "Adaptive remeshing for compressible flow computations", *Journal of Computational Physics,* Vol. 72, pp. 449-66, (1987);
[12] Peraire, J. and Peiró, J. and Morgan, K., "Finite element multigrid solution of euler flows past installed aero-engines", V.11.433-451, *J. Computational Mechanics*, (1993);
[13] Sorensen, K. A., Hassan, O., Morgan, K. and Weatherill, N. P., "An aglomeration unstructured hybrid mesh method for 2d turbulent compressible flows", *ISCFD'99*, Bremen, published in CD-ROM, (1999);
[14] Sorensen, K. A., *A multigrid procedure for the solution of compressible fluid flows on unstructured hybrid meshes,* Ph.D. thesis C/PH/251/01, University of Wales - Swansea, (2001);
[15] Sorensen, K. A. and Hassan, O. and Morgan, K. and Weatherill, N., "Agglomeration multigrid on hybrid meshes for compressible viscous flows", *ECCOMAS European Computational Fluid Dynamics Conference*, published in CD-ROM, (2001);
[16] TeCGraf– PUC-Rio: http://www.tecgraf.puc-rio.br;
[17] Zienkiewicz, O. C. and Morgan, K., *Finite element and approximation*, John Wiley & Sons, Inc., (1983).